



Performance of graphene hybrid-based ink for flexible electronics

D. S. Saidina^{1,2} · M. Mariatti¹ · S. A. Zubir¹ · S. Fontana² · C. Hérolde²

Received: 31 July 2019 / Accepted: 10 October 2019 / Published online: 15 October 2019
© Springer Science+Business Media, LLC, part of Springer Nature 2019

Abstract

The main aim of the present study is to develop graphene-based ink and graphene hybrid-based ink with excellent stability, physical and electrical properties for flexible electronics. Graphene foam (GF) was used as the graphene-like material and inkjet printing technique was utilized in the fabrication of the conductive patterns. GF ink, GF/poly(3,4-ethylenedioxythiophene) poly(styrenesulfonate) (PEDOT:PSS) hybrid ink and GF/silver nanoparticles (AgNPs) hybrid ink were prepared by using new mixed solvents of 2-propanol (IPA) and ethylene glycol (EG) at ratio of 1:1. Results showed that GF/PEDOT:PSS hybrid ink presented better stability and surface conductivity than those of GF ink and GF/AgNPs hybrid ink, in which the ink exhibited only 30% decrement from the initial concentration after a month and 100% improvement in the surface conductivity at 50 printed layers. Besides that, the conductive pattern made of GF/PEDOT:PSS hybrid ink exhibited gauge factor with the value of 4.3 which is capable to be used for low strain sensor application.

1 Introduction

Recently, flexible electronics are being used in nearly all kinds of electrical and electronic products. Flexible electronics can be an alternative to the rigid printed circuit board in certain applications because of the light weight, reduced thickness, ability to adapt various shapes, reduced time consumption and fabrication cost [1, 2]. Flexible electronics can be employed in a wide range of applications including sensors, touch screens, electronic paper, radio frequency tags, photovoltaic cells, light-emitting diodes, electronic textiles and etc. [3]. To date, flexible strain sensors fabricated using inkjet printing technique have received increasing attention over the conventional strain sensors due to the flexibility and relatively cost efficient [4, 5]. Graphene, a two-dimensional carbon nanomaterial has been widely utilized as a promising conductive material for conductive ink used in the inkjet printing replacing various nanomaterials and conductive polymers due to its remarkable electronic and mechanical properties [6, 7].

Moreover, researches on graphene hybrid-based inks by adding metallic nanoparticles or conductive polymers to improve the original properties of graphene for certain electronic applications have been widely developed. Several hybrid materials that been used by previous researchers are graphite nanoplatelets (GNPs) with polyaniline (PA), reduced graphene oxide (rGO) with silver nanoparticles (AgNPs), graphene oxide (GO) with AgNPs, Ag@gold nanotriangle platelets (AuNTPs) with GO, poly(3,4-ethylenedioxythiophene) (PEDOT) with rGO and gold nanoparticles (AuNPs) [8–14]. Table 1 presents a brief comparison between existing inks made of several types of hybrid materials. Most of graphene-based inks reported in the literature were prepared by using GO and GNPs as the graphene-like materials. However, GO sheets suffer from high number of oxygen-containing groups which reduced the electrical performance [15]. Post-treatment to reduce the functional groups in GO is required, however this process involved highly toxic materials such as hydrazine which are not environmentally friendly [16, 17]. Because of that, graphite nanoplatelets (GNPs) are used for graphene-based ink preparation as this material has good electrical properties. However, GNPs still shows poor solubility in common solvents and required treatment or stabilizer to improve the dispersion [16].

Graphene foam (GF), a three-dimensional interconnected network can be considered as the graphene-like material for the fabrication of graphene-based ink. GF is reported able

✉ M. Mariatti
mariatti@usm.my

¹ School of Materials and Mineral Resources Engineering,
Universiti Sains Malaysia, Engineering Campus,
14300 Nibong Tebal, Pulau Pinang, Malaysia

² Institut Jean Lamour, Campus Artem, 2 allée André Guinier,
BP 50840, 54011 Nancy Cedex, France

Table 1 Comparison between existing inks made of several types of hybrid materials

Hybrid ink	Sintering temperature (°C)	Sheet resistance/resistivity	Ref.
rGO/AgNPs	150 to 245	0.728 to $1.47 \times 10^{-5} \Omega \text{ cm}$	[9]
GO/AgNPs	400	$20 \Omega \text{ sq}^{-1}$	[10]
Ag@Au nanotriangular platelets/GO	Not available	$146.8 \Omega \text{ sq}^{-1}$	[12]
rGO/carbon black	100	0.09 M Ω	[13]
PEDOT:rGO/AuNPs	Not available	500 k $\Omega \text{ sq}^{-1}$	[14]

to avoid aggregation yet maintaining the electrical conductivity due to the interconnected network. GF has a porous structure and is a high surface area form of graphene can be synthesized via chemical vapour deposition and a solvothermal reaction method [18, 19]. So far, limited work has been done in the fabrication of GF as the conductive ink for printable flexible electronics. In the present study, graphene-based ink made of GF and graphene hybrid-based inks made of the combinations of GF with AgNPs and poly(3,4-ethylenedioxythiophene)-poly(styrenesulfonate) (PEDOT:PSS) were prepared. The effect of GF on the dispersion stability, viscosity, surface wettability, electrical properties and morphology of graphene-based ink and graphene hybrid-based inks were investigated.

2 Materials and methodology

2.1 Materials

Graphene foam (GF) with a density of 1.06 g cm^{-3} was prepared using a solvothermal reaction method according to the method reported by Speyer et al. [19]. This method involves three reaction steps, including solvothermal reaction, pyrolysis and washing. Anhydrous ethanol (Aldrich, > 99.8%) and metallic sodium were mixed together under inert atmosphere in a Parr autoclave with Nitrogen gas injected into the reactor. The autoclave was heated at 220°C for 72 h and the solvothermal product was sodium ethoxide. Sodium ethoxide was placed inside a vertical tubular oven and heated at 850°C for 4 h. The pyrolysis products contained carbon, sodium carbonate, sodium hydroxide and gaseous hydrocarbons. Finally, the pyrolysis products were washed with ethanol, hydrochloric acid and distilled water to remove sodium carbonate and sodium hydroxide, and then dried at 100°C for 24 h.

Silver nanoparticles (AgNPs) in powder form with a density of 10.49 g cm^{-3} and poly(3,4-ethylenedioxythiophene)-poly(styrenesulfonate) (PEDOT:PSS) conductive polymer

with a density of 0.985 g cm^{-3} supplied by Sigma Aldrich were used as hybrid materials in the production of graphene hybrid-based inks. Solvents including ethylene glycol (EG) ($\geq 99.5\%$) and 2-Propanol (IPA) ($\geq 99.8\%$) supplied by Merck KGaA, Darmstadt, Germany were used to disperse GF and GF hybrid in the preparation of conductive inks for inkjet printing. The flexible substrate used was polyethylene terephthalate (PET), manufactured by DuPont Mylar A with the thickness of $125 \mu\text{m}$ and opaque white appearance.

2.2 Methodology

The concentration of GF ink, GF/AgNPs hybrid ink and GF/PEDOT:PSS hybrid ink dispersed in IPA:EG mixed solvents at the ratio of 1:1 were fixed at 4 mg mL^{-1} . The formulations were sonicated at room temperature for an hour with 50% amplitude and 0.5 sonication cycle. Once the sonication was completed, GF ink and GF hybrid inks were collected. In this study, the printing layers were varied from 10 to 50 layers using Canon E510 series. Finally, the printed patterns were dried inside an oven at 100°C for 20 min. The schematic of flow work for the fabrication process of graphene-based ink pattern is shown in Fig. 1.

2.3 Characterization technique

The thickness and morphology of GF was characterized by using high resolution transmission electron microscopy (HRTEM, model FEI TECNAI G20).

The stability of GF ink and GF hybrid inks were investigated at their current pH via visual observation to evaluate the effectiveness of GF and GF hybrid dispersions and the stability of the resulting inks. All inks were observed and compared within a certain period of time. UV–Vis spectroscopy was performed by using a UV–Vis spectrophotometer, model Varian Cary 50 Conc, Agilent Technologies. The absorbance GF ink and GF hybrid inks were measured in-between 200 and 800 nm. The initial concentration of the conductive inks was fixed at 0.05 mg mL^{-1} and the supernatant of the conductive inks were used to obtain a detectable transmission during the measurements.

The zeta, ζ potential analysis is a well-known technique to evaluate the stability of a system by understanding the degree of electrostatic repulsion. The ζ -potential values were calculated based on the Helmholtz–Smoluchowski Eq. (1):

$$\xi = \frac{4\pi\mu v}{D} \quad (1)$$

where μ , v and D are the electrophoretic mobility, velocity and dielectric constant of the liquid at the boundary layer, respectively. In this study, ζ -potential of GF ink and GF hybrid inks were characterized by using a Zetasizer Nano

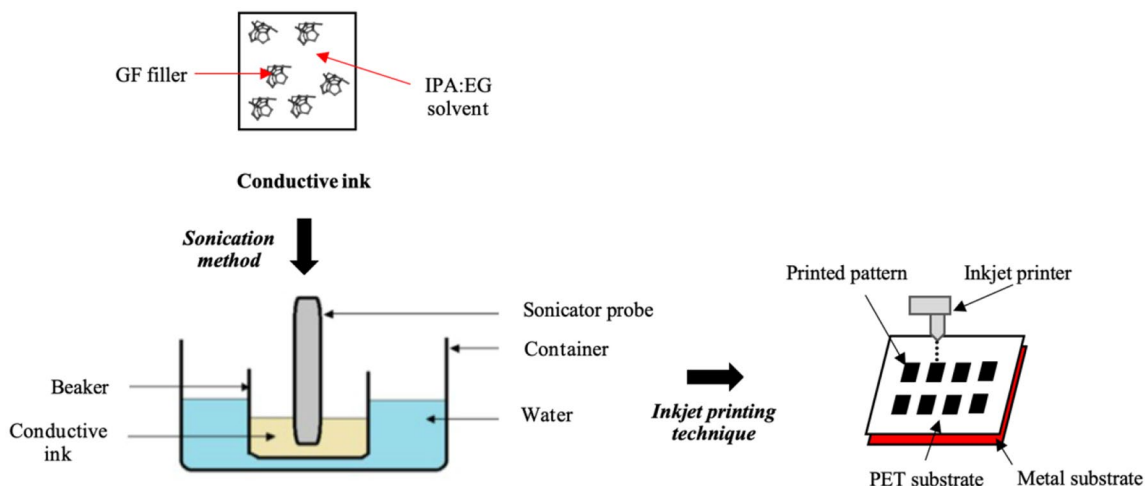


Fig. 1 Schematic of the fabrication process of graphene-based ink pattern using inkjet printing technique

Instrument, model Nano ZS ZEN3600, Malvern, UK. Three measurements consisting of 100 runs were performed for GF ink and GF hybrid inks, at current pH, and the average results were reported.

The ink viscosity, η was measured by a cone and plate rheometer at the shear rate within a range of 1–500 s^{-1} using a model Physica MCR 301, Anton Paar Malaysia Sdn. Bhd. The contact angle, θ_c was measured by the sessile drop method with a droplet volume of 5 μL using a goniometer, model Rame hart Instrument. Co, USA on the PET substrate. DROPimage Advanced software was used to obtain the contact angle. The morphology of the printed patterns was characterized by using scanning electron microscopy (SEM) model QUANTA FEG450.

The tensile test was performed to investigate the mechanical behavior of printed ink on the substrate, and therefore confirm their suitability for flexible interconnects. In this study, the strain sensing characteristics were tested by using a mechanical Instron 3366 tensile testing machine with a crosshead speed of 1 mm min^{-1} and uniform strain/release cycle of 5%, 10% and 20%, respectively.

The gauge factor is defined as the ratio of per unit change in resistance to the per unit change in length and can be calculated using Eq. 2.

$$\text{GaugeFactor} = \frac{\frac{\Delta R}{R_0}}{\frac{\Delta L}{L_0}} \quad (2)$$

where $\frac{\Delta R}{R_0}$, $\frac{\Delta L}{L_0}$ and gauge factor are per unit change in resistance, per unit change in length and gauge factor, respectively.

3 Results and discussion

3.1 Morphology of GF

Figure 2 illustrates the high resolution transmission electron microscopy (HRTEM) images of GF particle. It is observed that GF consists of folded edges almost throughout the GF structure and nine parallel lines could be observed, an early indication that it was a multi-layer graphene. The interlayer distance for GF was 0.33 nm.

3.2 Stability of GF ink, GF/AgNPs and GF/PEDOT:PSS hybrid inks

Visual observation of GF ink, GF/AgNPs and GF/PEDOT:PSS hybrid inks at concentration of 4 mg mL^{-1} observed from day 1 (after sonication) until day 7 was shown in Fig. 3. For GF ink (Fig. 3a), small amount of settling was observed at day 7 indicated that GF is partially stable up to a week. On the other hand, GF/AgNPs hybrid ink was only stable for 1 day as the hybrid ink appeared clearer at day 7. Sedimentation of high amounts of GF and AgNPs were observed at the bottom of the bottle at day 7, indicating the dispersion of GF and AgNPs in IPA:EG solvents were not stable. This is attributed to the high interfacial tension between GF ($\sim 40 \text{ mJ m}^{-2}$) and AgNPs ($\sim 7.2 \text{ J m}^{-2}$) and also, the high density of AgNPs (10.49 g cm^{-3}) that leads to poor stability of the dispersion [20]. However for GF/PEDOT:PSS hybrid ink, it can be seen that the hybrid ink was visually homogeneous with dark appearance even until day 7, indicating that the dispersion of GF hybrid with

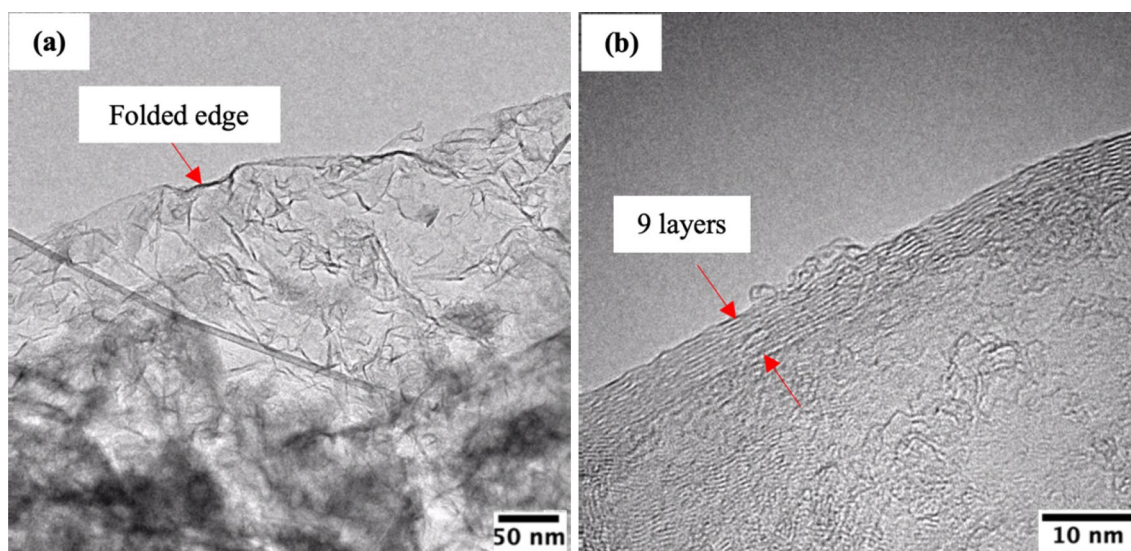


Fig. 2 HRTEM micrographs of GF particle at magnifications of **a** 97 kX and **b** 690 kX

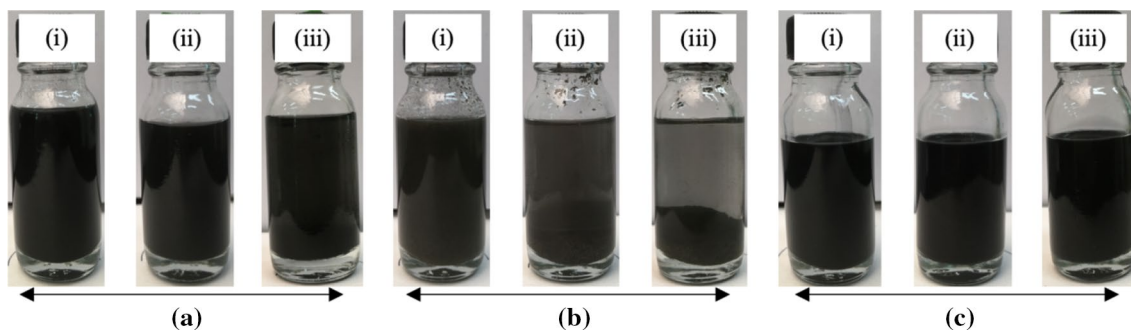


Fig. 3 Photographs of **a** GF ink, **b** GF/AgNPs hybrid ink and **c** GF/PEDOT:PSS hybrid ink. (i), (ii) and (iii) refer to the image after sonication (day 1), day 3 and day 7, respectively

PEDOT:PSS in IPA:EG mixed solvents was stable for a long period. Low interfacial tension between GF ($\sim 40 \text{ mJ m}^{-2}$) and PEDOT:PSS ($\sim 42.5 \text{ mJ m}^{-2}$) leads to good stability of the hybrid ink dispersion [21].

UV–Vis spectroscopy was used to analyze the quality, nature and the stability of GF ink and GF hybrid inks. The UV–Vis absorption spectra of GF ink and GF hybrid inks are shown in Fig. 4. As seen from Fig. 4a, the highest absorption peak for GF ink was observed at 265 nm which attributed to the π – π^* transition of the C–C aromatic ring in the GF ink [22].

The formation of AgNPs and PEDOT:PSS in GF hybrid inks were confirmed by the absorption peaks in the UV–Vis spectra, as shown in Fig. 4b and c, respectively. As clearly seen, GF/AgNPs hybrid ink had absorbance peak at 418 nm, showing a peak associated with surface plasmon resonance of AgNPs. Saion et al. [23] and Campillo et al. [24] reported a maximum peak of AgNPs lies in between 404 to 418 nm. Meanwhile for GF/PEDOT:PSS ink, the maximum

absorption was observed at 227 nm which refers to the aromatic rings of PSS [25, 26].

The dispersion stability of GF and GF hybrid inks in IPA:EG mixed solvents were investigated by measuring their concentrations for a month, as illustrated in Fig. 5. The concentration of GF and GF hybrid inks were evaluated at 660 nm using Lambert–Beer's equation; $A = \alpha CL$, where A , α , C and L are the absorbance, absorption coefficient with the value of $2460 \text{ mL mg}^{-1} \text{ m}^{-1}$, concentration of the conductive ink and cell length, respectively [27, 28]. Based on the calculated concentrations, GF/PEDOT:PSS hybrid ink shows a slight decrement after 1 month (30%) as compared to those of GF ink and GF/AgNPs hybrid ink with the percentage decrement of 50% and 70%, respectively. From this observation, GF/PEDOT:PSS hybrid ink was stable than those conductive inks. This result is parallel with the visual observation which has been discussed in Fig. 3.

Table 2 presents concentration decrement and zeta, ζ potential values of GF and GF hybrid inks. According to

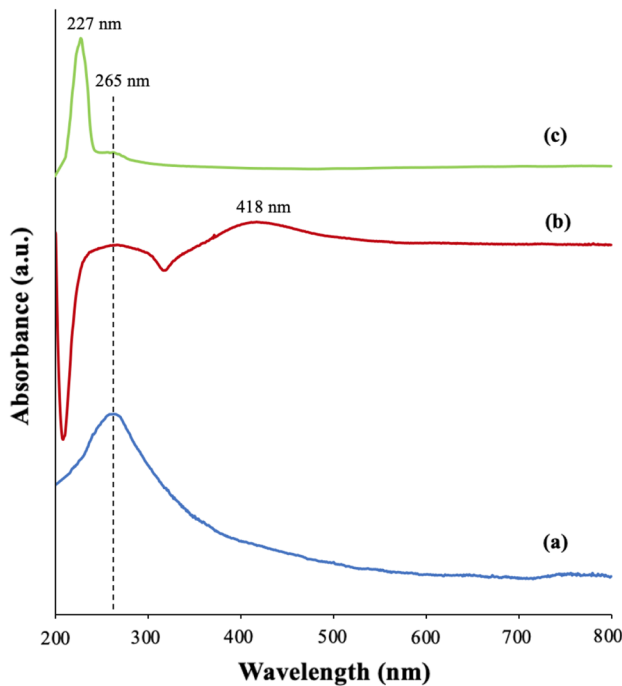
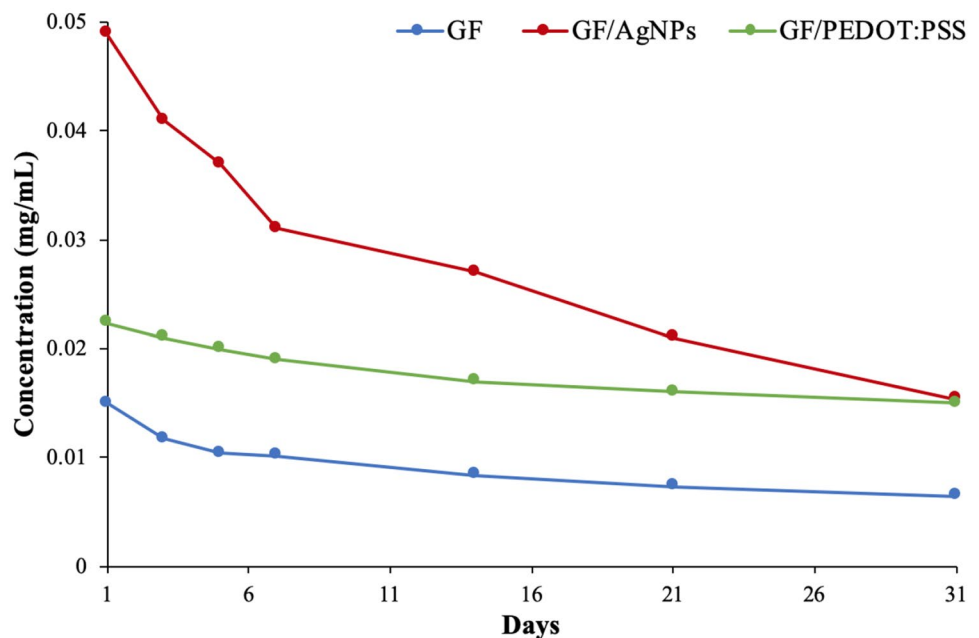


Fig. 4 UV-Vis absorption spectra of **a** GF, **b** GF/AgNPs hybrid ink and **c** GF/PEDOT:PSS hybrid ink

Rajan et al. [29], the optimum values for good stabilization of nano dispersion when the ζ -potential is more than 30 mV or less than -30 mV, indicating highly charged particles which prevent aggregation of the particles due to electric repulsion. The ζ -potentials values of GF ink, GF/AgNPs hybrid ink and GF/PEDOT:PSS hybrid ink were less than -30 mV. GF/PEDOT:PSS hybrid ink exhibited the lowest

Fig. 5 Concentration of GF ink, GF/AgNPs hybrid ink and GF/PEDOT:PSS hybrid ink as a function of time



ζ -potential with the value of -80.4 mV as compared to other conductive inks, indicating that this hybrid ink has the best stability than GF ink and GF/AgNPs hybrid ink, respectively. Zeta potential results in Table 2 generally support the results shown by visual observation and UV-Vis analysis.

3.3 Physical properties of GF ink, GF/AgNPs and GF/PEDOT:PSS hybrid inks

Table 3 presents viscosity, η contact angle, θ_c and surface energy, γ_{SL} values of GF and GF hybrid inks. The η for all inks range between 7.5 and 11.9 mPa s, indicating that all inks are acceptable for inkjet printing. Figure 6 illustrates the η curves of GF ink and GF hybrid inks. The η for GF ink and GF hybrid inks decreased with increasing shear rate, indicating pseudoplastic (shear-thinning flow) behavior. Shear-thinning is a phenomenon in which the viscosity of the conductive ink decreases with increasing shear stress. This phenomenon is suitable to be used in inkjet printing where the conductive ink has high viscosity under standard conditions but low viscosity when passing through the print head in order to avoid nozzle clogging [30].

According to Khondoker et al. [31], the surface wettability of the conductive ink with the substrate play an important role which significantly influence the printing quality. The measured values of the θ_c and γ_{SL} of GF ink and GF hybrid inks on the PET substrate are shown in Table 3. Based on Table 3, it was found that the θ_c for hybrid inks is slightly increased with an addition of hybrid material; AgNPs and PEDOT:PSS. However, the θ_c is still below 90° , which is considered as good adhesion between conductive ink and the PET substrate. The

Table 2 Concentration decrement and zeta potential of GF and GF hybrid inks

Ink	Concentration decrement (%)	Zeta potential (mV)
GF	50	−38.9
GF/AgNPs	70	−50
GF/PEDOT:PSS	30	−80.4

Table 3 Comparison physical properties of GF and GF hybrid inks

Ink	Viscosity (mPa s)	Contact angle (°)	Surface energy (mJ m ^{−2})
GF	7.5	32.9	41.1
GF/AgNPs	9.8	33	41.1
GF/PEDOT:PSS	11.8	37.3	39.4

images of a drop of conductive ink dispensed from the goniometer on the substrate are shown in Fig. 7. The γ_{SL} from the measured θ_c of GF ink and GF hybrid inks range in between 39.4 to 41.1 mJ m^{−2}, resulting the tendency of

GF ink and GF hybrid inks to become less reactive with the surrounding.

3.4 Electrical properties of printed GF ink and GF hybrid inks

Figure 8 shows the printed GF and GF hybrid inks on PET substrate at different number of printing layers. As expected based on Fig. 8, the color of the printed patterns became darker with an increasing of printing layers, especially for GF/PEDOT:PSS hybrid ink. However for GF ink and GF/AgNPs hybrid ink, the printed color were less darker as compared to GF/PEDOT:PSS hybrid ink. It is believed that the printed sample with darker color has better connection and might influence the electrical properties. Denneulin et al. [32] reported that as the number of printing layers increased, the conductive film became connected to each other and therefore increased the electrical properties.

The conductive ink patterns made of GF ink and GF hybrid inks at different printing layers were fabricated using inkjet printing in order to determine the conductivity behavior. Figure 9a, b presents the surface conductivity of GF ink and GF hybrid inks as a function of printing layer. As

Fig. 6 Viscosity curves of (a) GF ink, (b) GF/PEDOT:PSS hybrid ink and (c) GF/AgNPs hybrid ink as a function of shear rate

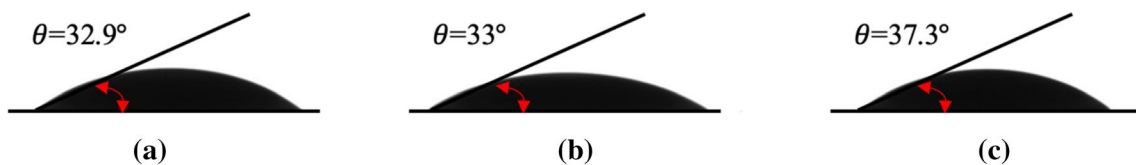
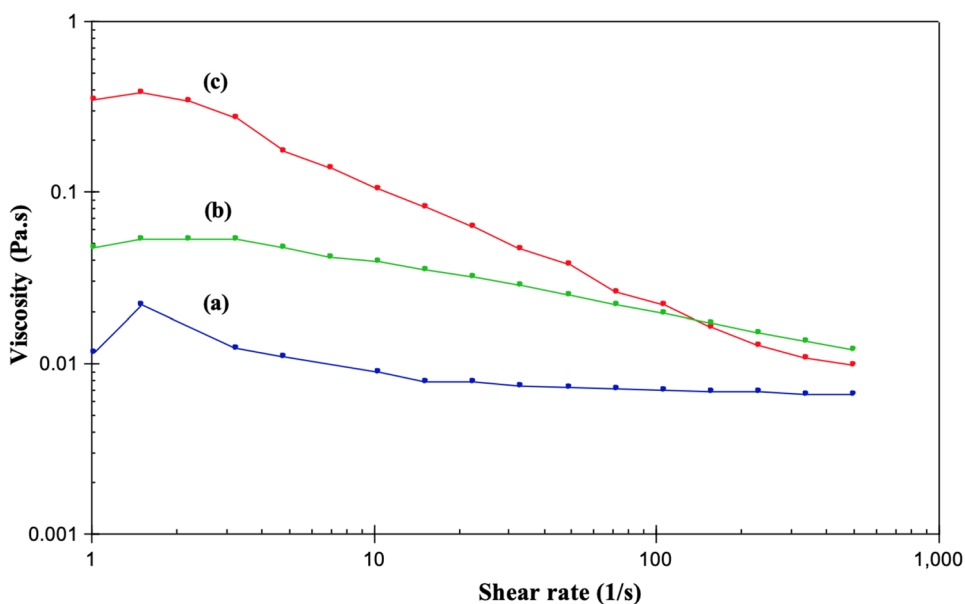
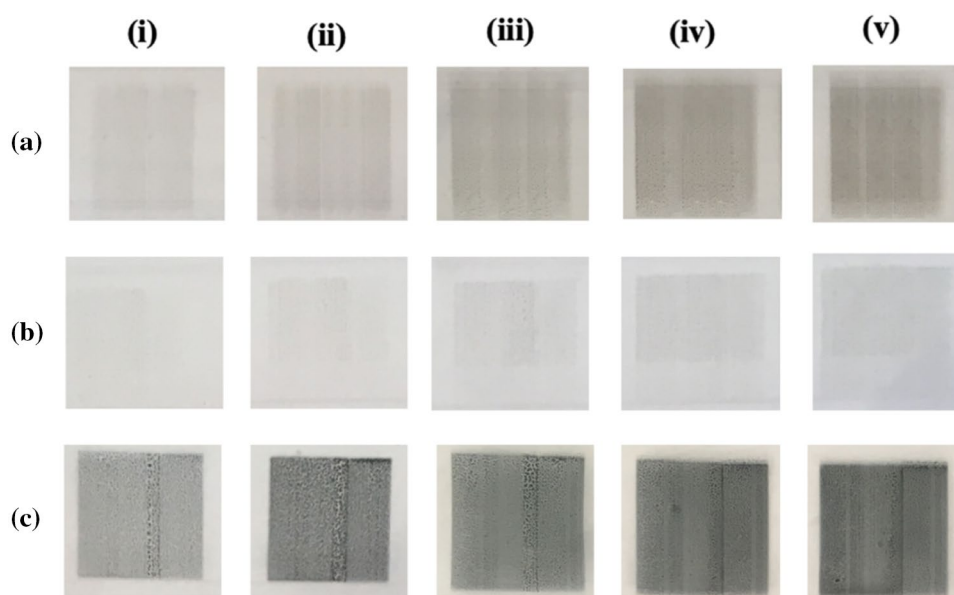


Fig. 7 The droplet of a GF ink, b GF/AgNPs hybrid ink and c GF/PEDOT:PSS hybrid ink

Fig. 8 Photographs of printed **a** GF ink, **b** GF/AgNPs hybrid ink and **c** GF/PEDOT:PSS hybrid ink on PET substrate with different printing layers (i) 10 layers, (ii) 20 layers, (iii) 30 layers, (iv) 40 layers and (v) 50 layers



clearly seen, the surface conductivity of the printed patterns for all samples increased evidently with increasing printing layer. Conductive ink made of GF/PEDOT:PSS hybrid shows the highest surface conductivity compared to those of GF ink and GF/AgNPs hybrid ink at all printing layers. GF/PEDOT:PSS hybrid ink exhibited remarkable improvement of surface conductivity from 10 printing layers to 50 printing layers, followed by GF/AgNPs hybrid ink and GF ink by 100%, 55% and 54%, respectively.

Even though the electrical conductivity of pure GF and AgNPs were higher than pure PEDOT:PSS, there is also other factors that influenced the surface conductivity of the printed patterns mainly including the ink stability. Dang et al. [33] reported that the conductive ink should be stable at least during the printing process. As discussed in Sect. 3.2, GF/PEDOT:PSS shows the best stability amongst all conductive inks. Poor ink stability may lead to several problems during printing process which include nozzle clogged and conductive material trapped on the ink cartridge filter, as shown in Fig. 10. Figure 10a, b shows nozzle clogged and conductive material trapped on the ink cartridge filter due to poor ink stability. This results to poor printing quality and therefore affected the surface conductivity of the printed patterns as discussed in Fig. 9.

Besides that, the surface conductivity of the printed patterns is completely influenced by their morphology. Figure 11 shows the morphology of the top printed surface of GF ink and GF hybrid inks with respect to the printing layer that provides information of conductive network formation. Figure 11a–d shows the conductive paths were not connected and spread randomly over the substrate showing that amount of GF and GF/AgNPs hybrid were not sufficient to support complete network. Meanwhile for

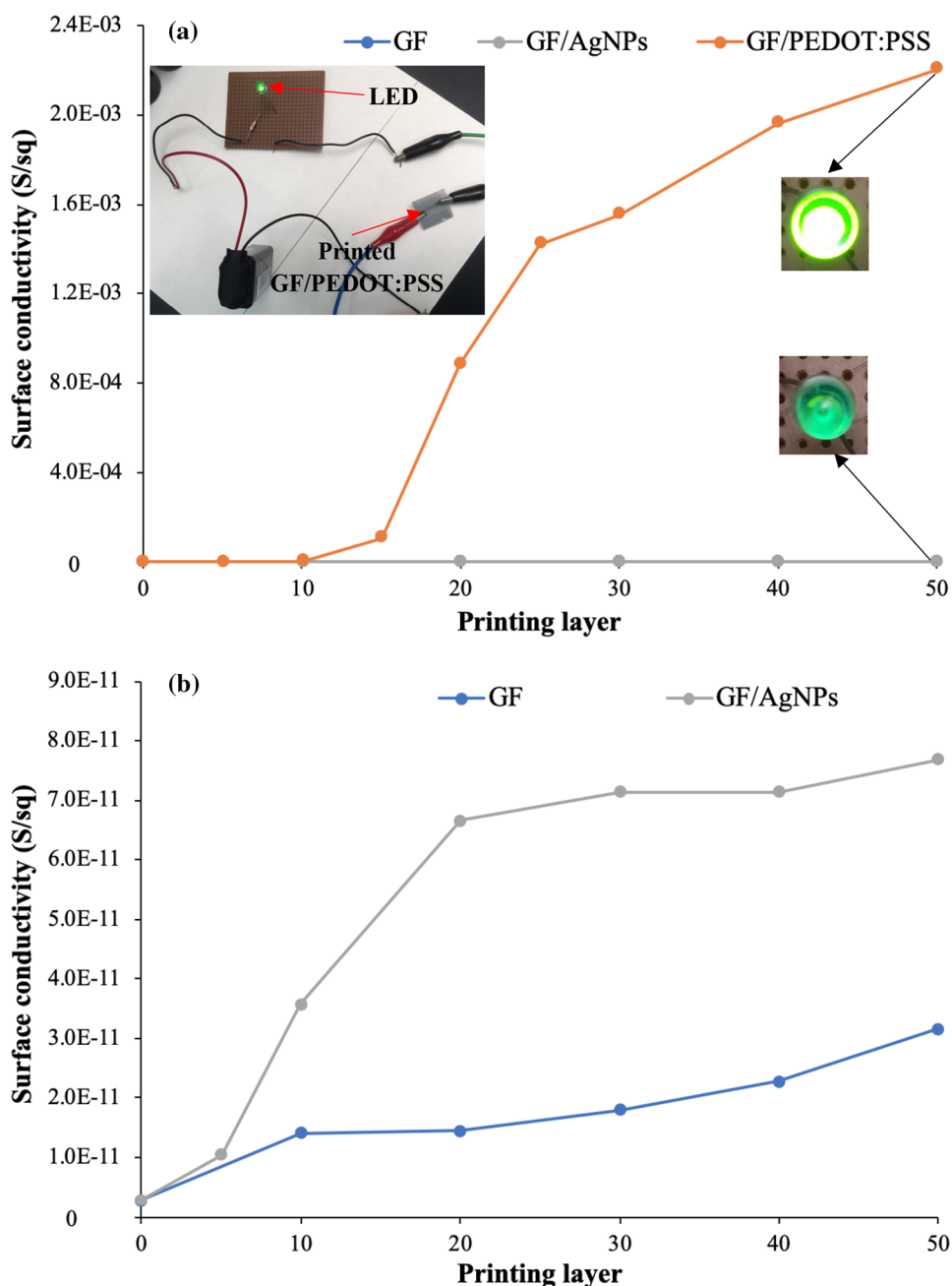
GF/PEDOT:PSS hybrid (Fig. 11e, f), the network become denser and the conductive network was fully formed. The continuity of the printed patterns improved with an increasing of printing layer from 10 layers to 50 layers. The printed quality of the conductive inks improved as the number of printing layer increased. This observation is in accordance with the previous report by Gao et al. [34] on the fabrication of graphene patterns on the glass substrate using inkjet printing method.

3.5 GF/PEDOT:PSS hybrid ink for strain sensor

Based on the results shown in the previous sections, GF/PEDOT:PSS hybrid ink was selected for strain sensor characterization. Figure 12 presents the typical curves for the relative change of resistance of GF/PEDOT:PSS hybrid sensor. Different strain levels of $\epsilon = 1\%$, 2% and 3% were applied to GF/PEDOT:PSS hybrid printed sensor. The resistance was fully recovered for stretch/release cycles with maximum strain, $\epsilon = 3\%$. It is observed that the linearity of sensor at 1% is slightly better than those of sensor at 2% and 3% strain, respectively. Linearity has an important role for the strain sensor, as it enables the strain rate to be obtained more easily as soon as the resistance change is known. Good linearity means that the resistance change was gentle with sensor stretching [35]. Non-linearity of sensor makes the calibration process complex and difficult [36].

As shown in Fig. 12, the relative change resistance of the strain for GF/PEDOT:PSS hybrid sensor was fully recovered to its original value after the stress being released from 1% up to 3% . The findings indicated the recovery performance and hysteresis behavior of the printed hybrid sensor. This results in the motion detection more accurate and reliable.

Fig. 9 **a** Surface conductivity of GF ink and GF hybrid inks as a function of printing layer and **b** enlargement of surface conductivity of GF ink and GF/AgNPs hybrid ink, inset showing digital images of an electronic circuit set up and LED brightness for printed GF ink and GF hybrid inks



Small hysteresis was observed during $\epsilon = 1\%$. Meanwhile, large hysteresis behavior could be seen when the printed sample was applied at $\epsilon = 3\%$. Large hysteresis behavior leads to the irreversible sensing performance sensor upon dynamic load [37]. Based on the hysteresis curve, the performance of GF/PEDOT:PSS hybrid sensor at low strain 1% is better than those at high strain of 2% and 3%, respectively.

Table 4 compares the values of gauge factor calculated in the present study with the previous works. The strain sensor produced in the present study exhibited gauge factor of 4.3 with strain range of 0–20%. Higher gauge factor value is required for the strain sensor due to its high sensitivity. Based

on the comparison, it is observed that the sensitivity gauge factor of the strain sensor based GF/PEDOT:PSS obtained in the present study is higher compared to those of previous works reported by Correia et al. [38] and Borghetti et al. [39] but lower than Casiraghi et al. [40]. The prepared hybrid sensor has the capability to be used for low sensitive strain sensing application.

Fig. 10 Photographs of ink cartridge problems due to poor stability including **a** nozzle clogged and **b** conductive ink trapped on the ink cartridge filter; in comparison with **c** no conductive material trapped on the cartridge filter

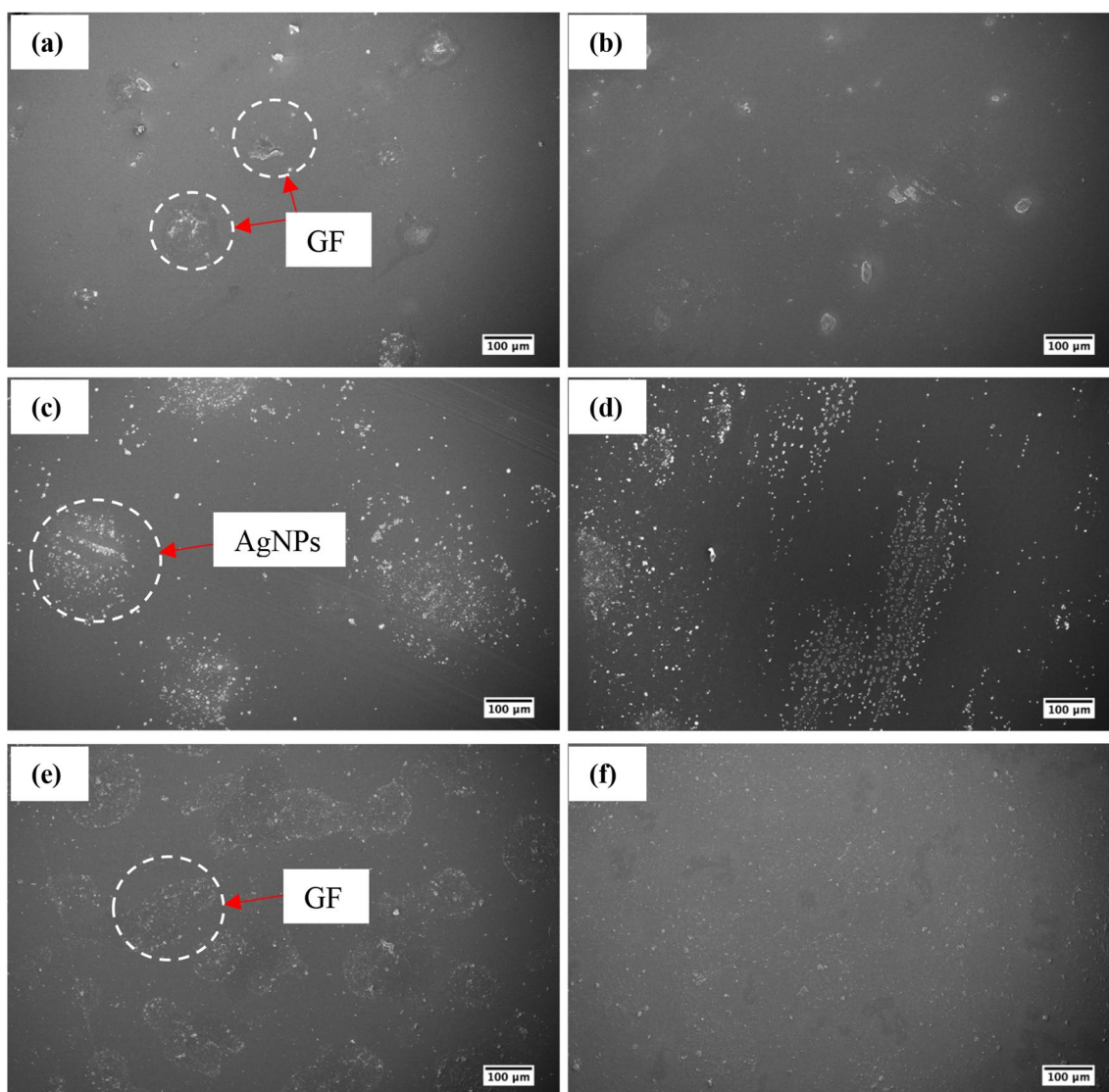
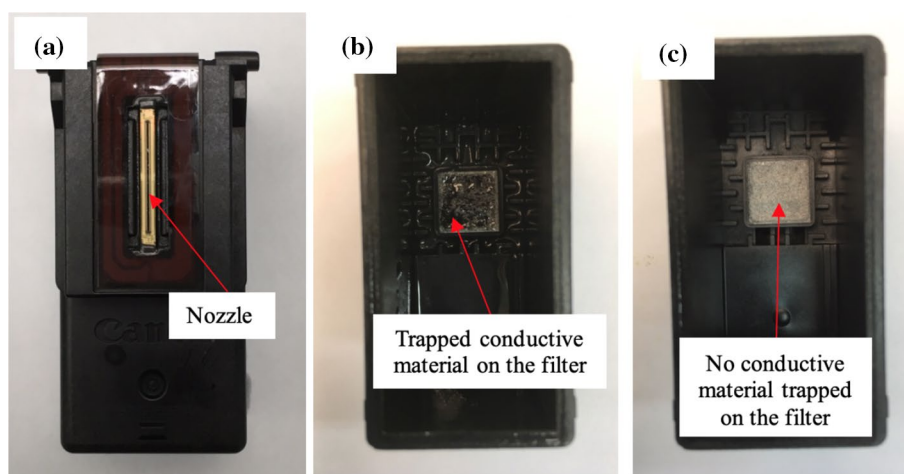


Fig. 11 SEM micrographs of top printed surface made of **a, b** GF ink, **c, d** GF/AgNPs hybrid ink and **e, f** GF/PEDOT:PSS hybrid ink at **a, c, e** 10 printing layers and **b, d, f** 50 printing layers ($\times 100$ mag.)

Fig. 12 Relative change resistance and hysteresis behavior of GF/PEDOT:PSS hybrid sensor as a function of strain, inset showing digital image of a tensile test set up for printed GF/PEDOT:PSS hybrid sensor

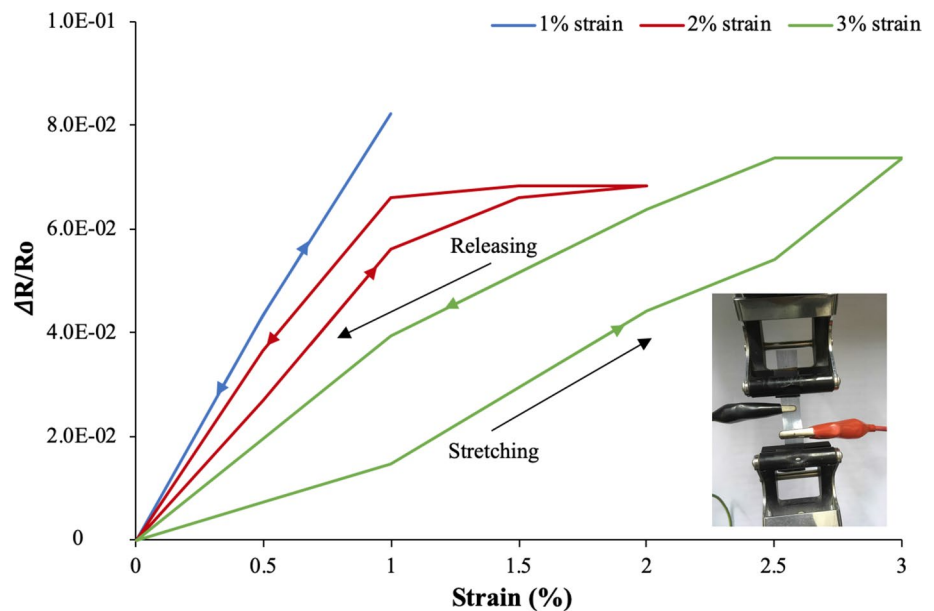


Table 4 Comparison of gauge factor between present study and from literature

Materials	Gauge factor	Strain range (%)	Ref.
GF/PEDOT:PSS	4.3	0–20	Present study
PEDOT	2.48	Not mentioned	[38]
Ag	0.35	Not mentioned	[38]
PEDOT:PSS	<1	Not mentioned	[39]
Ag	3.7	Not mentioned	[39]
Graphene	125	20	[40]

4 Conclusions

In this work, graphene-based ink and graphene hybrid-based inks were successfully fabricated. Results showed that GF/PEDOT:PSS hybrid ink has better stability than those of GF ink and GF/AgNPs hybrid ink with slight decrement from its concentration after a month with the values of 30%, 50% and 69%, respectively. Also, conductive ink made of GF/PEDOT:PSS hybrid exhibits 100% improvement of surface conductivity from 10 printing layers to 50 printing layers compared to those of 55% and 54% shown by GF/AgNPs hybrid and GF, respectively. Strain sensor made of printed GF/PEDOT:PSS hybrid was prepared and exhibits gauge factor with the value of 4.3 and strain range of 0–20%.

Acknowledgements The authors gratefully acknowledge the financial support from the Ministry of Education Malaysia and Fundamental Research Grant Scheme (FRGS) for granting the research fund used for this project (Project No. 6071385). The authors gratefully acknowledge also the support from the School of Materials & Mineral Resources Engineering, Universiti Sains Malaysia. We were also grateful to Carbon Materials Group (E205)'s laboratory, Institut Jean Lamour,

Université de Lorraine, France for the research attachment of the first author at Université de Lorraine, France.

References

1. W.C. Leong, M.Z. Abdullah, C.Y. Khor, *Microelectron. Reliab.* **53**, 1996–2004 (2013)
2. K. Shen, X. Chen, M. Guo et al., *Sensors Actuators B* **105**, 251–258 (2005)
3. F. Torrisi, T. Hassan, W. Wu et al., *ACS Nano* **6**, 2992–3006 (2012)
4. A.M. Gaikwad, D.A. Steingart, T. Nga Ng et al., *Appl. Phys. Lett.* **102**, 104 (2013)
5. C. Cochrane, V. Koncar, M. Lewandowski et al., *Sensors* **7**, 473–492 (2007)
6. S.H. Bae, Y. Lee, B.K. Sharma et al., *Carbon* **51**, 236–242 (2013)
7. H. Tian, Y. Shu, Y.L. Cui et al., *Nanoscale* **6**, 699–705 (2014)
8. Y. Xu, I. Hennig, D. Freyberg et al., *J. Power Sources* **248**, 483 (2014)
9. W. Yang, C. Wang, V. Arrighi et al., *J. Mater. Sci. Mater. Electron.* **28**, 8218 (2017)
10. D. Deng, S. Feng, M. Shi et al., *J. Mater. Sci. Mater. Electron.* **28**, 15411 (2017)
11. W. Zhang, E. Bi, M. Li et al., *Colloids Surf. A* **490**, 232 (2016)
12. L. Li, M. Gao, Y. Guo et al., *J. Mater. Chem. C* **5**, 2800 (2017)
13. A. Ji, Y. Chen, X. Wang et al., *J. Mater. Sci. Mater. Electron.* **29**, 13032 (2018)
14. R. Zhang, B. Peng, Y. Yuan, *Compos. Sci. Technol.* **168**, 118 (2018)
15. L. Huang, Y. Huang, J. Liang et al., *Nano Res.* **4**, 675–684 (2011)
16. T.S. Tran, N.K. Dutta, N.R. Choudhury, *Adv. Colloid Interface Sci.* **261**, 41–61 (2018)
17. S. Pei, H.M. Cheng, *Carbon* **50**, 3210–3228 (2012)
18. G. Ning, C. Xu, Y. Cao et al., *J. Mater. Chem. A* **1**, 408–414 (2013)
19. L. Speyer, S. Fontana, S. Cahen et al., *Solid State Sci.* **50**, 42–51 (2015)
20. K.K. Nanda, A. Maisels, F.E. Kruijs et al., *Phys. Rev. Lett.* **91**, 106102 (2003)

21. P. Dabczyński, M.M. Marzec, Ł. Pięta et al., *ACS Omega* **3**, 3631–3639 (2018)
22. F.T. Johra, J.W. Lee, W.G. Jung, *J. Ind. Eng. Chem.* **20**, 2883–2887 (2014)
23. E. Saion, E. Gharibshahi, K. Naghavi, *Int. J. Mol. Sci.* **14**, 7880–7896 (2013)
24. G.E. Campillo, E. Vélez, G. Morales et al., *J. Phys: Conf. Ser.* **850**, 012023 (2017)
25. D.A. Mengistie, M.A. Ibrahim, P.C. Wang et al., *ACS Appl. Mater. Interfaces.* **6**, 2292–2299 (2014)
26. J. Saghaei, A. Fallahzadeh, M.H. Yousefi, *Org. Electron.* **19**, 70–75 (2015)
27. U. Khan, A. O'Neill, M. Lotya et al., *Small* **6**, 864–871 (2010)
28. M. Lotya, P.J. King, U. Khan et al., *ACS Nano* **4**, 3155–3162 (2010)
29. K. Rajan, I. Roppolo, A. Chiappone et al., *Nanotechnol. Sci. Appl.* **9**, 1–13 (2016)
30. C. O'Mahony, E.U. Haq, C. Silien et al., *Micromachines (Basel)* **10**, 99 (2019)
31. M.A.H. Khondoker, S.C. Mun, J. Kim, *Appl. Phys. A* **112**, 411–418 (2013)
32. A. Denneulin, J. Bras, A. Blayo et al., *Nanotechnology* **20**, 385701 (2009)
33. M.C. Dang, T.M.D. Dang, E. Fribourg-Blanc, *Adv. Nat. Sci. Nanosci. Nanotechnol.* **4**, 015009 (2013)
34. Y. Gao, W. Shi, W. Wang et al., *Ind. Eng. Chem. Res.* **53**, 16777–16784 (2014)
35. S. Shengbo, L. Lihua, J. Aoqun et al., *Nanotechnology* **29**, 255202 (2018)
36. B.U. Hwang, J.H. Lee, T.Q. Trung et al., *ACS Nano* **9**, 8801–8810 (2015)
37. C.X. Liu, J.W. Choi, *Microelectron. Eng.* **117**, 1–7 (2014)
38. V. Correia, C. Caparros, C. Casellas et al., *Smart Mater. Struct.* **22**, 105028 (2013)
39. M. Borghetti, M. Serpelloni, E. Sardini et al., *Sensors Actuators A* **243**, 71–80 (2016)
40. C. Casiraghi, M. Macucci, K. Parvez et al., *Carbon* **129**, 462–467 (2018)

Publisher's Note Springer Nature remains neutral with regard to jurisdictional claims in published maps and institutional affiliations.